# STATE OF THE CLIMATE IN 2015

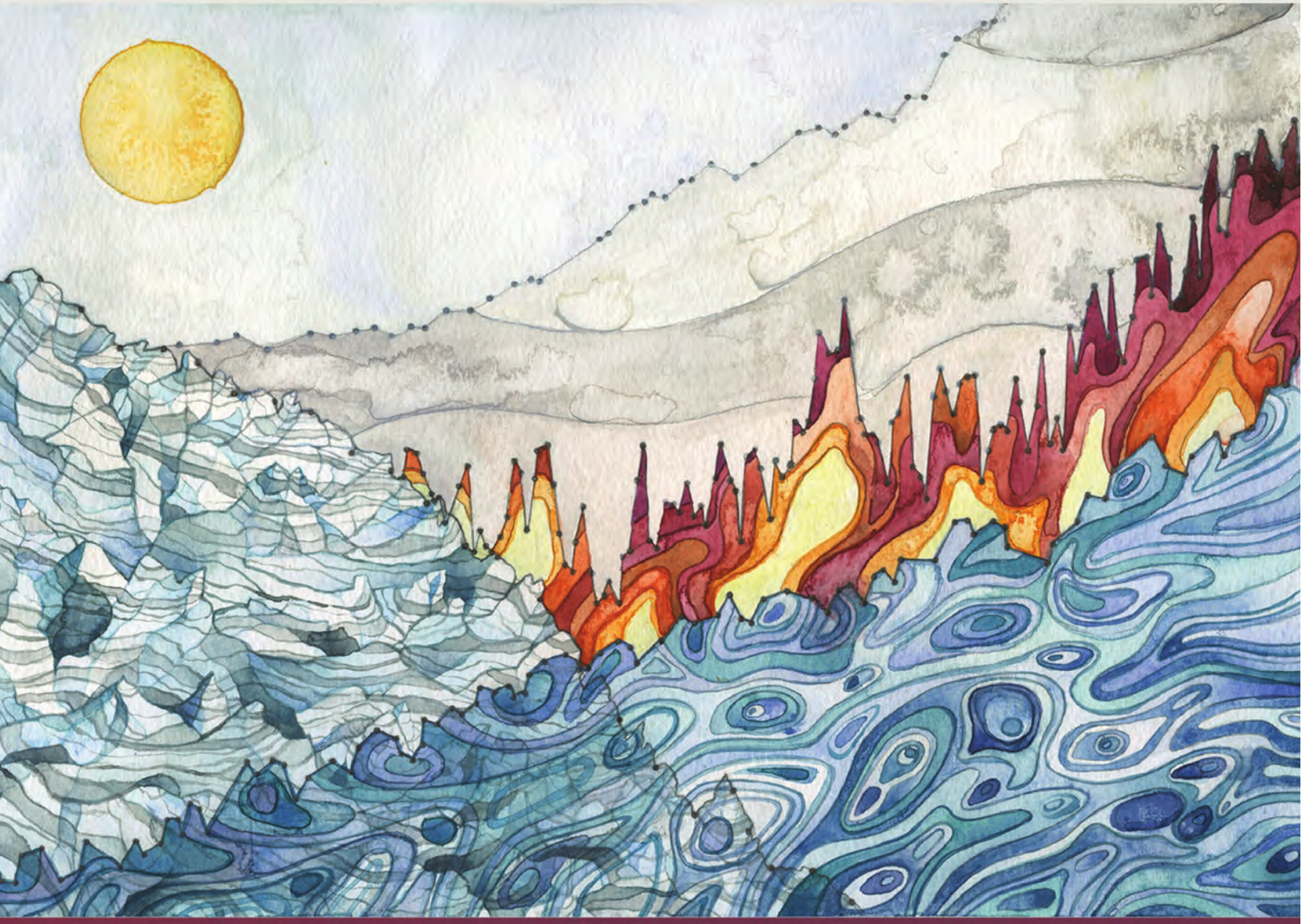

Special Supplement to the
*Bulletin of the American Meteorological Society*
Vol. 97, No. 8, August 2016

where ozone columns were largely below average (Plate 2.1q). The strong negative anomalies at high Southern Hemisphere latitudes reflect the large Antarctic ozone hole observed in September–December, whose size reached maximum values that were near the all-time record high (see section 6h).

In Fig. 2.46 the total ozone annual means from different data sources are shown for 1970–2015 in various zonal bands: near-global (60°S–60°N), midlatitudes in both hemispheres (35°–60°), and the inner tropics (20°S–20°N). Also shown are the polar time series in March (Northern Hemisphere, 60°–90°N) and October (Southern Hemisphere, 60°–90°S), the months when polar ozone losses are largest in each hemisphere. Poleward of 60°S, a record low October mean was observed (Fig. 2.46e). Weaker-than-usual dynamical wave activity in the Southern Hemisphere winter diminished transport from the tropics, reducing ozone at Southern Hemisphere midlatitudes and in the collar region of the polar vortex, and permitting a very stable and cold polar vortex. The high vortex stability and low temperatures resulted in larger-than-usual polar ozone losses and a near-record ozone hole in terms of size and persistence. Ozone annual mean columns at mid- to polar latitudes (35°–90°) in each hemisphere are largely determined by winter/spring ozone levels. These vary considerably with changes in stratospheric meteorological conditions (e.g., Steinbrecht et al. 2011; Weber et al. 2011; Kuttippurath et al. 2015). The year-to-year variability seen in all ozone time series also reflects quasi-biennial oscillation (QBO)-related variations extending from the tropics into the extratropics (Randel and Wu 1996; Strahan et al. 2015).

It is clear that the Montreal Protocol and its Amendments have been successful in stopping the multidecadal decline in stratospheric ozone by the late 1990s (WMO 2011). However, at most latitudes, it has not yet been possible to determine a statistically significant increase in total column ozone or lower stratosphere ozone because the expected small increases are masked by large interannual variability (e.g., Chehade et al. 2014; Coldewey-Egbers et al. 2014; Frith et al. 2014; Kuttippurath et al. 2015; Nair

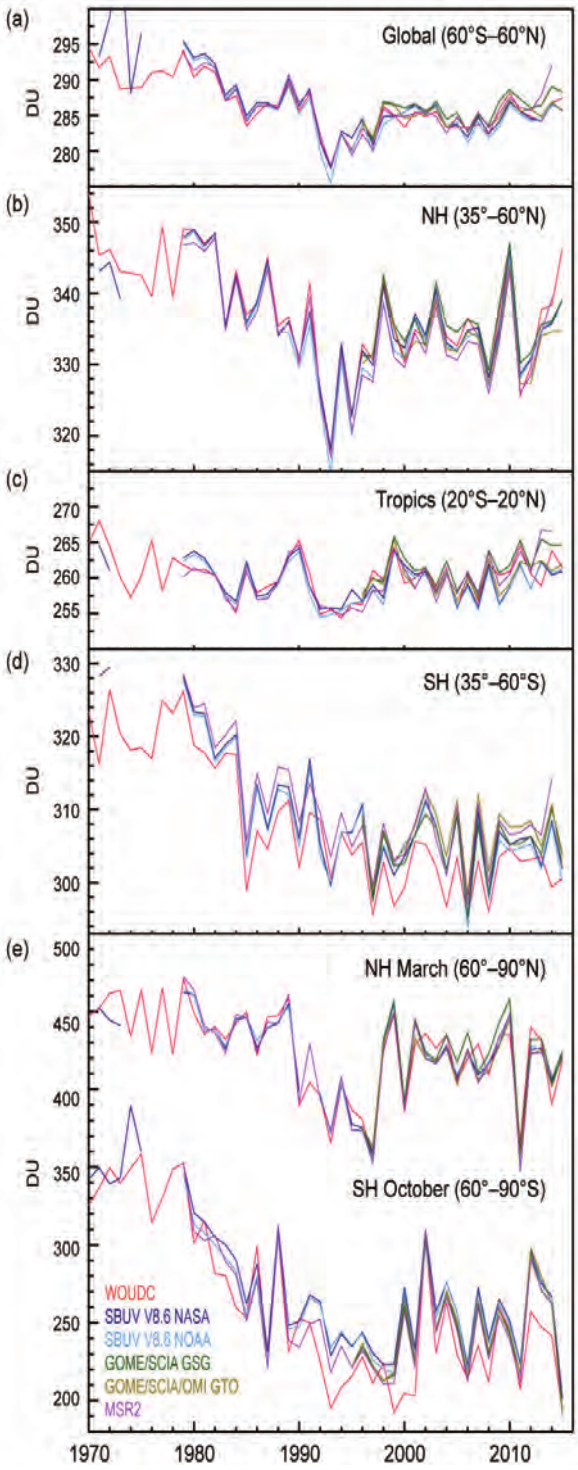


**Fig. 2.46. Time series of annual mean total ozone in (a–d) four zonal bands and (e) polar (60°–90°) total ozone in Mar (Northern Hemisphere) and Oct (Southern Hemisphere). Data are from WOUDC ground-based measurements combining Brewer, Dobson, SAOZ, and filter spectrometer data (red: Fioletov et al. 2002, 2008); the BUV/SBUV/SBUV2 V8.6 merged products from NASA (MOD V8.6, dark blue, Chiou et al. 2014; Frith et al. 2014) and NOAA (light blue, Wild et al. 2012); the GOME/SCIAMACHY/GOME-2 products GSG from University of Bremen (dark green, Weber et al. 2011) and GTO from ESA/DLR (light green, Coldewey-Egbers et al. 2015); and the MSR V2 assimilated dataset extended with GOME-2 data (van der A et al. 2015). WOUDC values for 2015 are preliminary because not all ground station data were available in early 2016.**

et al. 2015; de Laat et al. 2015). The 2015 total ozone columns in Fig. 2.46 are consistent with this overall picture and lie within the expected usual variations.

In the tropics, no discernible long-term trends in total column ozone have been observed for the entire 1970–2015 period (see Fig. 2.46). Ozone trends in the tropical lower stratosphere are mainly determined by tropical upwelling (related to changes in sea surface temperature). In a changing climate it is expected that tropical upwelling will increase and thus ozone will continue to decline (Zubov et al. 2013; WMO 2014). However, there is some evidence of a hiatus in tropical upwelling trends and corresponding lower stratospheric ozone trends during the last decade (Aschmann et al. 2014). Because tropospheric ozone contributes to the total ozone columns, trends in total ozone, despite major contributions from the lower stratosphere, may differ from trends in lower stratospheric ozone (Shepherd et al. 2014).

The most recent ozone assessment (WMO 2014) and studies (Nair et al. 2015; Harris et al. 2015) indicate that the clearest signs of significant ozone increases should occur in the upper stratosphere (2%–4% decade$^{-1}$ at ~2 hPa or 40 km; see Fig. 2.47). However, there still are uncertainties associated with the various available data records and with the proper interpretation of statistical approaches used to derive and attribute trends (e.g., Nair et al. 2015; Kuttippurath et al. 2015; Harris et al. 2015). This is reflected in the updated Stratospheric Aerosol and Gas Experiment (SAGE)–Optical Spectrograph and Infrared Imager System (OSIRIS) record, which now better accounts for tangent altitude drifts, and in the updated Solar Backscatter Ultraviolet (SBUV) data from NOAA with improved inter-satellite adjustments. Overall, the 2015 annual means in Fig. 2.47 support the claim of recent increases in upper stratospheric, extra-polar ozone. These suggest the Montreal Protocol has successfully turned the previous downward trend in ozone into an ozone increase, at least in the upper stratosphere.

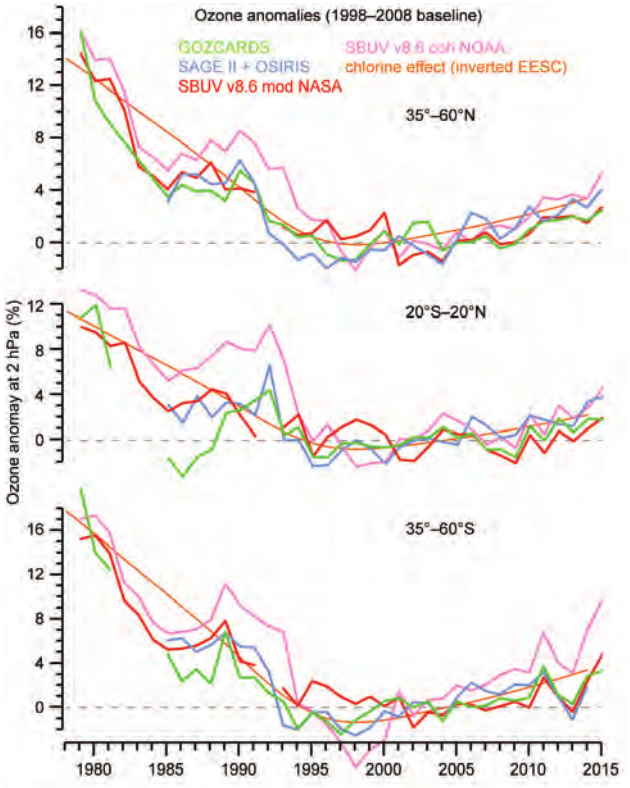


**Fig. 2.47. Annual mean ozone anomalies at 2 hPa (~40 km, upper stratosphere) in three zonal bands. Data are from the merged SAGE II/OSIRIS (Bourassa et al. 2014) and GOZCARDS (Froidevaux et al. 2015) records and from the BUV/SBUV/SBUV2 v8.6 merged products from NASA (McPeters et al. 2013; Frith et al. 2014) and NOAA (Wild et al. 2012) (base period: 1998–2008). The orange curves represent EESC (effective equivalent stratospheric chlorine), scaled to reflect the expected ozone variation due to stratospheric halogens. Data points for 2015 are preliminary, because SAGE-OSIRIS data were not yet available after July 2015, and adjusted SBUV2 v8.0 data are used after July 2015 instead of v8.6 data, which are not available in early 2016.**

5) Stratospheric water vapor—S. M. Davis, K. H. Rosenlof, D. F. Hurst, and H. B. Selkirk

Variations in stratospheric water vapor (SWV) over interannual-to-decadal timescales have the potential to affect stratospheric ozone (Dvortsov and Solomon 2001) and surface climate (Solomon et al. 2010). Throughout the first 10 months of 2015, water vapor mixing ratios in the tropical lowermost stratosphere were within 10% (0.4 ppm, μmol mol$^{-1}$) of the previous decade's average. Then, starting in November and continuing through December, tropical lowermost SWV increased to near-record levels, especially over the tropical western Pacific and Indian Ocean regions. The deep tropical-averaged (15°S–15°N) SWV anomaly at 82 hPa, based on data from the *Aura* Microwave Limb Sounder (MLS), was +0.7 ppm (+17%) in November and +0.9 ppm (+24%) in December. These values are in stark contrast to the weak negative (dry) tropical average anomalies of about −0.2 ppm (−6%) in November–December 2014 (Figs. 2.48, 2.49). Since the MLS record began in August 2004, the November–December 2015 anomalies at 82 hPa are surpassed only by +0.9 ppm (+25%) deep tropical anomalies in February–March 2011. The +0.7 ppm (+19%) average deep tropical anomaly at 100 hPa in November–December 2015 is the high-

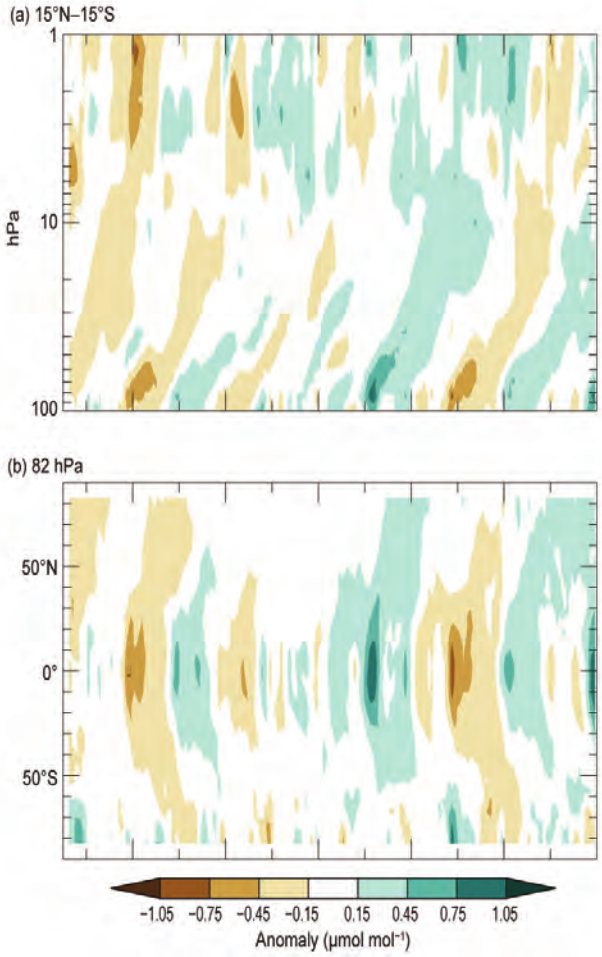


**Fig. 2.48. (a) Vertical profiles of MLS tropical (15°S–15°N) water vapor anomalies (μmol mol$^{-1}$) and (b) latitudinal distributions of MLS water vapor anomalies (μmol mol$^{-1}$) at 82 hPa. Anomalies are differences from the 2004–15 mean water vapor mixing ratios for each month.**

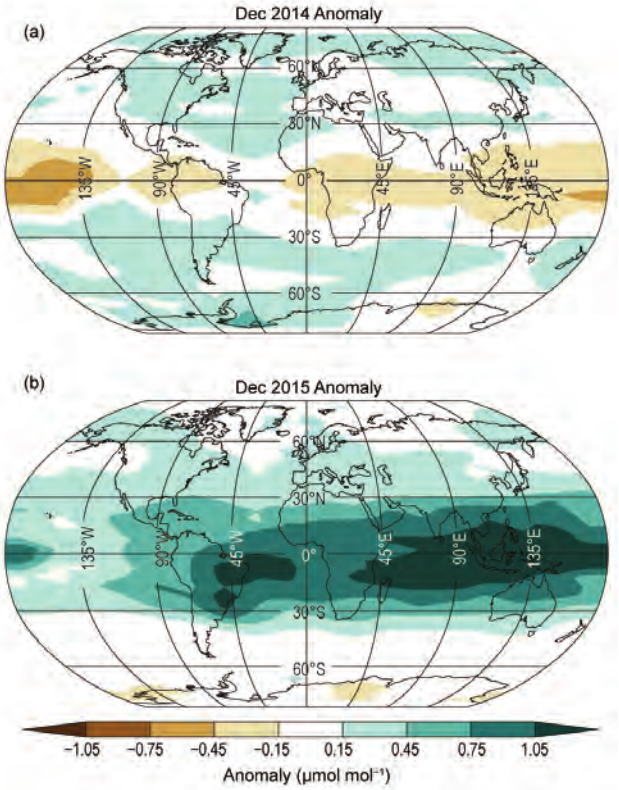


**Fig. 2.49. Global stratospheric water vapor anomalies (μmol mol$^{-1}$) centered on 82 hPa in (a) Dec 2014 and (b) Dec 2015 from the *Aura* Microwave Limb Sounder.**

est ever observed by MLS at that pressure level. The change in tropical lower SWV from December 2014 to December 2015 was +1.1 ppm, ~50% of the typical seasonal mixing ratio amplitude at 82 hPa in the tropics. Strong water vapor increases in the tropical lower stratosphere at the end of 2015 were also observed at Hilo, Hawaii (20°N), and San José, Costa Rica (10°N), by balloonborne frost point hygrometers (Figs. 2.50b,c).

The seasonal variability of water vapor in the tropical lower stratosphere is predominantly controlled by the annual cycle of cold-point temperatures (CPTs) in the tropical tropopause layer (TTL). These minimum temperatures determine the amounts of water vapor that remain as moist tropospheric air masses are freeze-dried during their slow ascent into the stratosphere. Seasonal-to-interannual variations in tropical lower SWV are highly correlated with CPT variations in the TTL. The dramatic increase in tropical lower SWV at the end of 2015 is consistent with the observed ~1°C increase in tropical CPTs over the same period (Fig. 2.50c).

Interannual variations in CPTs are potentially related to the changing phases of the El Niño–Southern Oscillation (ENSO) and the stratospheric quasi-biennial oscillation (QBO). In October, the QBO phase transitioned from easterly (cold) to westerly (warm) and persisted in the westerly phase through the end of 2015 (see sections 2b3, 2e3). The evolution towards a warmer TTL and wetter tropical lower stratosphere at the end of 2015 is consistent with this reversal of the QBO phase. Regionally, the enhancement of SWV in the tropical western Pacific and Indian Ocean regions is consistent with the adiabatic response of the TTL to reduced convection in this region as a result of the El Niño conditions present during 2015. Other factors such as variations in the strength of the Brewer–Dobson circulation can also impact SWV anomalies on an interannual timescale. However, given the potential interrelationships between ENSO, QBO, and the Brewer–Dobson circulation, a rigorous attribution of the positive SWV anomalies present at the end of 2015 is not possible.

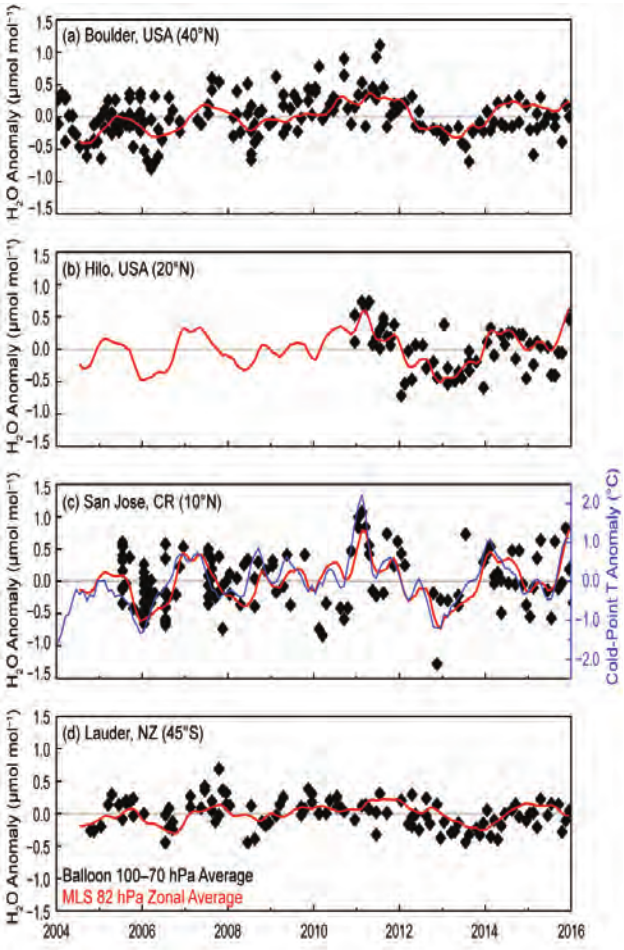


**Fig. 2.50. Lower stratospheric water vapor anomalies (μmol mol$^{-1}$) at 82 hPa over four balloonborne frost point (FP) hygrometer stations. (a)–(d) show the anomalies of individual FP soundings (black) and of monthly zonal averages of MLS retrievals in the 5° latitude band containing the FP station (red). High-resolution FP vertical profile data were averaged between 70 and 100 hPa to emulate the MLS averaging kernel for 82 hPa. Each MLS monthly zonal mean was determined from 2000 to 3000 profiles. Tropical cold-point temperature anomalies based on the MERRA reanalysis [(c), blue curve] are generally well correlated with the tropical lower SWV anomalies.**

Anomalies in tropical lower SWV propagate from the tropics to the midlatitudes of both hemispheres, as is visually demonstrated by the many "C"-shaped contours in Fig. 2.48b. The late 2015 wet anomaly in tropical lower SWV (Figs. 2.48b, 2.50c) was just starting to reach the midlatitudes of each hemisphere at the end of 2015.

During 2015, SWV anomalies over Lauder, New Zealand, were close to zero or slightly positive (Fig. 2.50d). These are consistent with the poleward transport of weak dry tropical SWV anomalies present at the end of 2014 and early 2015 (Fig. 2.49a), and the 2014 Antarctic vortex being anomalously weak, warm, and less dehydrated (Davis et al. 2015; see sections 2b3 and 6h). In general, Southern Hemisphere midlatitude SWV can vary interannually with the degree of seasonal dehydration within the Antarctic vortex and the strength of the poleward transport of dehydrated air masses (Fig. 2.48b). Indeed, the 2015 Antarctic vortex was particularly strong (see section 6h), as evidenced by the appearance of a −0.5 ppm anomaly in the high southern latitudes near the end of 2015 (Fig. 2.48b).

### 6) Tropospheric ozone—J. R. Ziemke and O. R. Cooper

Two of the most important reasons to monitor tropospheric ozone are that it is a surface pollutant with harmful biological effects and is a greenhouse gas that affects long-term climate change. Tropospheric ozone is also the primary source of the hydroxyl radical (OH), the main oxidizing agent for pollutants in the troposphere. Sources of tropospheric ozone include transport from the stratosphere, photochemical production from lightning $NO_x$, and photochemical production from precursor gases emitted by the combustion of fossil fuels, biofuels, and biomass (e.g., Sauvage et al. 2007; Martin et al. 2007; Leung et al. 2007; Murray et al. 2013; Hess and Zbinden 2013; Young et al. 2013).

The variability of tropospheric ozone, from urban to hemispheric scales, is driven by a combination of photochemical ozone production and atmospheric transport. Tropospheric ozone production varies because its precursor gases and sunlight are variable. Transport phenomena that drive large-scale variability include ENSO (e.g., Chandra et al. 1998, 2009; Sudo and Takahashi 2001; Doherty et al. 2006; Koumoutsaris et al. 2008; Voulgarakis et al. 2011) and the Madden–Julian oscillation (MJO: Sun et al. 2014). Small- to large-scale tropospheric ozone variability also occurs over shorter periods, including weekly baroclinic timescales (e.g., Ziemke et al. 2015, and references therein), and finer scale airstream transport on the order of hours to days. Changes in tropospheric ozone at hemispheric and global scales include decadal trends (e.g., Hess and Zbinden 2013; Cooper et al. 2014; Lin et al. 2014; Parrish et al. 2014).

Global maps of annual means and anomalies of tropospheric column ozone from the satellite-based Ozone Monitoring Instrument (OMI) and MLS for 2015 are shown in Fig. 2.51 and Plate 2.1u, respectively. As in previous reports, OMI/MLS ozone trends are calculated only for latitudes 60°S–60°N where there is full annual coverage by OMI. In 2015, as for the last decade, annual average tropospheric column ozone

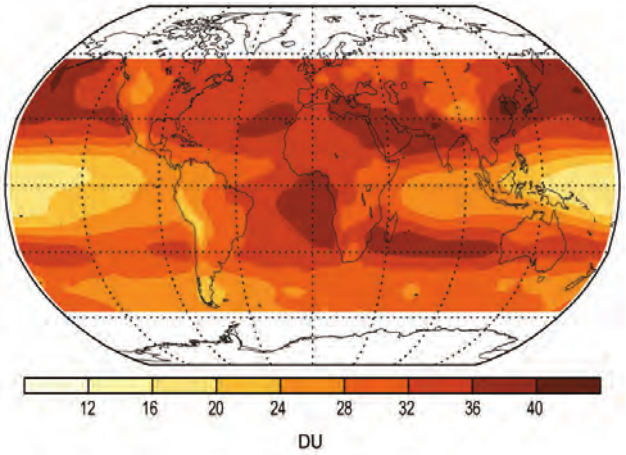


**Fig. 2.51. Average OMI/MLS tropospheric ozone column ozone for 2015. Data poleward of ±60° are not shown due to the inability of OMI to measure ozone during polar night.**

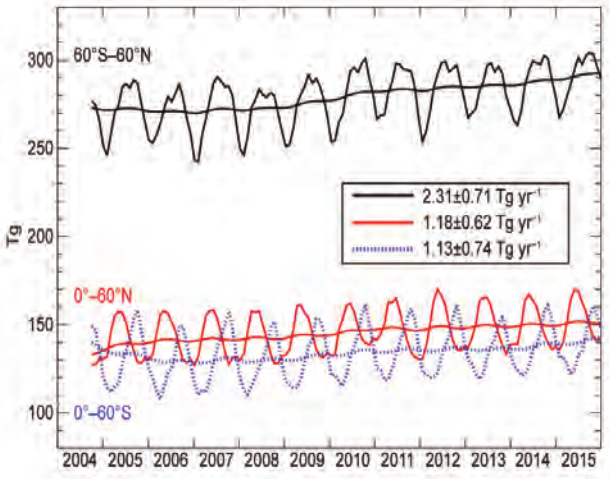


**Fig. 2.52. Monthly averages of OMI/MLS tropospheric ozone burdens (Tg) from Oct 2004 through Dec 2015. The top curve (black) shows 60°S–60°N monthly averages with 12-month running means. The bottom two curves show monthly averages and running means for the Northern Hemisphere (red) and Southern Hemisphere (blue). Slopes of linear fits (Tg yr$^{-1}$) of all three curves are also listed along with their ±2σ statistical uncertainties.**

amounts in the Northern Hemisphere exceeded those in the Southern Hemisphere. Some basic features of tropospheric column ozone include strong topographical effects, such as greatly reduced amounts over the Tibetan Plateau and the western U.S. Rocky Mountain region, with much larger amounts east and west of these regions over both land and ocean. The greatest annual mean tropospheric column values were observed over the Mediterranean–South Asian region and from eastern China eastward toward North America. In the tropics, the west-to-east zonal wave-1 pattern (Fishman et al. 1990) is evident, with high values over the Atlantic and low values over the Pacific. An extended band of high ozone was present at 30°S, with the greatest amounts between southern Africa and Australia. Zonally-averaged tropospheric column averages and their 95% confidence intervals for 2015 were 30.7 ± 2.2 DU for 60°S–60°N, 32.1 ± 2.6 DU for 0°–60°N, and 29.4 ± 1.9 DU for 0°–60°S. These column averages convert to tropospheric burdens of 291.2 ± 20.9, 152.1 ± 12.3, and 139.1 ± 9.0 Tg, (Tg = $10^{12}$ g), respectively. For comparison, the tropospheric column averages for 2005–15 for the three regions were 29.5 ± 2.1, 30.7 ± 2.5, and 28.2 ± 2.2 DU (279.0 ± 19.9, 145.4 ± 11.8, and 133.6 ± 10.4 Tg).

The 2015 average tropospheric ozone burdens for each hemisphere and the globe were greater than those in 2014, and 12-month running averages of each show steady increases since October 2004 (Fig. 2.52). Linear trends (in Tg yr$^{-1}$) with their ± 2σ statistical uncertainties are also given. The increasing trends in OMI/MLS tropospheric column ozone are statistically significant for both hemispheric means and the near-global mean. Relative to the average burdens for 2005–15 the three trends all depict increases of 0.8% yr$^{-1}$. The combined OMI/MLS record now exceeds 11 years and the measured increases are becoming more indicative of true long-term trends, building on similar findings from previous reports.

Cooper and Ziemke (2013) reported surface ozone increasing since 1990 over eastern Asia and the western United States, but decreasing over the eastern United States, using measurements by ground- and satellite-based instruments. Cooper and Ziemke (2014) presented a time series of near-global (60°S–60°N) tropospheric burdens determined from satellite measurements that indicated a statistically significant increase over 2005–13 and Cooper and Ziemke (2015) showed that the increase in global tropospheric ozone continued through 2014.

For the past two years, the *State of the Climate* tropospheric ozone summary was based upon only the OMI/MLS satellite measurements (Ziemke et al. 2006) due to insufficient updated analyses of the ground-based measurement network data since 2012. Updates of the surface ozone data and trends have continued to be infrequent during 2015, so once again only the OMI/MLS satellite data are used. One significant change from previous reports is the use of new MLS version 4.2 ozone retrievals. A new activity of the International Global Atmospheric Chemistry (IGAC) project began in earnest in 2015 to produce a Tropospheric Ozone Assessment Report (TOAR). The TOAR is expected to be completed by the end of 2016 and will summarize the global distribution